ELSEVIER

Nuclear Instruments and Methods in Physics Research B 171 (2000) 277–290

NIM B
Beam Interactions with Materials & Atoms

www.elsevier.nl/locate/nimb

Inferring ejection distances and a surface energy profile in keV particle bombardment experiments

A. Delcorte [a,*], B.G. Segda [b,1], B.J. Garrison [a], P. Bertrand [b]

[a] *Department of Chemistry, Penn State University, 152 Davey Lab, University Park, PA 16802-6300, USA*
[b] *Unité de Physico-Chimie et de Physique des Matériaux, Université Catholique de Louvain, 1 pl. Croix du Sud, B-1348 Louvain-la-Neuve, Belgium*

Received 23 March 2000; received in revised form 2 May 2000

Abstract

The disappearance cross-sections and kinetic energy distributions of fragment ions sputtered from polystyrene thin films under 12 keV $^{69}Ga^{+}$ ion bombardment are measured using a time-of-flight spectrometer. Even though the disappearance cross-sections are often used as an indicator of radial ion beam damage, the derived radii range from 2 to 10 Å depending on the particular hydrocarbon fragment. Therefore, the disappearance cross-sections cannot be directly related to a single global quantity of damage per incident particle. Likewise, the widths of the measured kinetic energy depend on the particular hydrocarbon fragment. Both the disappearance cross-sections and the widths of the kinetic energy distribution superficially relate to fragment mass but the correlation is not perfect. We develop a hypothesis that the disappearance cross-section and the width of the kinetic energy distribution actually correlate with the ejection radius of the particular fragment. Thus, the kinetic energy distributions provide an estimate of the radial extent of the energy density in the ejection region. Our interpretations are supported by molecular dynamics simulation results. For comparison with previously reported data, our results indicate that the deposited energy profile is 4–5 times narrower than for 72.3 MeV, electronic sputtering of PVDF [Phys. Rev. Lett. 77 (1996) 667].

Keywords: Secondary ion mass spectrometry; Sputtering; Ion emission; Kinetic energy distribution; Ion induced damage; Disappearance cross-section; Polymer; MD simulation

1. Introduction

When an energetic primary ion interacts with an organic surface, atoms, small hydrocarbon fragments and characteristic molecular segments are sputtered in a neutral or charged state [2,3]. The mass-separation of the charged sputtered species constitutes the basis of secondary ion mass

* Corresponding author. Tel.: +1-814-863-2108; fax: +1-814-863-5319.
E-mail address: delcorte@chem.psu.edu (A. Delcorte).
[1] Permanent address: Département de Physique, Faculté des Sciences et Techniques, Université de Ouagadougou, BP 7021 Ouagadougou 03, Burkina Faso.

0168-583X/00/$ - see front matter
PII: S0168-583X(00)00263-9

spectrometry (SIMS) [4]. In organic SIMS, the complex peak pattern contained in the mass spectrum is used to identify the molecular species present in the topmost layer of the sample, crucial information in many processes involving surfaces and interfaces. Currently, the range of applications of organic SIMS is indeed wide, going from automotive paints to compact disks, or from molecular solids of amino acids to frozen cells and tissues [5,6]. Given the importance of the applications, efforts have been made towards understanding the essential physics and, consequently, the basic processes leading to the emission and ionization of polyatomic fragments are starting to become unraveled.

One of the intriguing questions in the sputtering of organic species is which portion of the energy of the primary beam gives rise to ejection of molecules and fragments and how this energy is distributed around the particle impact. In this respect, the knowledge of the local energy density associated with the ejection of different fragments would constitute an interesting part of the answer. The above question also relates to the issue of beam induced damage in organic samples. At first sight, one might think that the disappearance cross-section (σ), deduced from dynamic experiments, should indicate the average extent of the damaged area, but the experimental results show that σ is not constant for various fragments. From a slightly different perspective, it is tempting to interpret the disappearance cross-section as the average area from which the corresponding fragment is emitted, but again we must make sure that no other factors strongly affect σ. We are also interested to know the influence of the primary projectile (downward motion) in the fragmentation process, which should be reflected by the distribution of distances between the impact and the ejected fragments. In this paper, our aim is to shed some light on the relationships between energy deposition at the surface, fragmentation and secondary particle ejection in the case of organic overlayers bombarded by primary ions with several kiloelectronvolts of energy. In particular, we wish to establish the profile of the energy distributed around the point of impact of the primary projectile and its relation to the sputtered species observed in the SIMS spectrum. For this purpose, we think it is prudent to combine two different but complementary approaches, i.e., SIMS experiments and molecular dynamics (MD) simulations. Polystyrene (PS), a standard polymer, is used as a model molecule throughout this study.

More than 15 years ago, Benninghoven [7,8] proposed the precursor concept as an interesting approach to address the above-mentioned issues. The concept was initially developed for organic monolayers on metals, but some of the features should be valid for bulk organic systems. In [7], he depicted a view of the energy distribution at the surface induced by keV particle bombardment, and its relation with the ejection of intact and fragmented molecules. In order to check the model, the same group designed several experiments to measure the distribution $E(r)$ of the collision cascade energy, averaged over many bombardment events [9,10]. Although the information provided in the performed experiments is somewhat indirect, it gives a good idea about the shape of $E(r)$ for organic molecules adsorbed on metals. The effort involved to achieve these measurements is certainly remarkable since a direct microscopic observation of $E(r)$ appears impossible by experimental means.

Recently, a clever experimental procedure has been developed by Papaleo et al. [1] to measure the same quantity $E(r)$ for the MeV bombardment of a poly(vinylidene fluoride) (PVDF) film. In this study, the kinetic energy of the sputtered species is correlated to an estimate of their mean ejection radius around the impact point. The ejection radius is deduced from dynamic ion beam degradation measurements. The relevance of this approach is supported by several arguments. First, the ejected species must somehow mirror the state of the damaged region created at the surface by the bombardment. Moreover, the rate of the secondary ion intensity decay during ion-beam induced degradation experiments should indicate the extent of the disturbed area at the surface. Second, the internal and kinetic energies of the sputtered ions should directly relate to the fast energy transfer leading to their emission and to the distribution of the impact energy on the sample surface. Nevertheless, the meaning of the correlation between the

two sets of data originating from these static (energy distributions) and dynamic measurements (degradation rates) is not completely clear.

Theoretically, the application of MD simulations to keV particle bombardment of solids has provided valuable insights into the sputtering mechanisms of organic overlayers, owing to the use of realistic many-body potentials [11–13]. The emission of characteristic fragments from polystyrene molecules has been successfully modeled [14]. In particular, it has been shown that the emission of PS fragments like C_3H_3, C_6H_5 and C_7H_7 is mostly induced by the initial interaction between the primary particle and the PS chain, without any significant influence of the collision cascade that develops later in the substrate. This mechanism is certainly valid over a wide range of primary particle energies, i.e., from 150 eV to 5 keV. The nature of this process constitutes a good reason to believe that the formation of short PS fragments, if not their yield, is almost independent of the substrate nature and of the organic layer thickness. Therefore, we want to use these new simulation results to complement the information provided by SIMS experiments and to support our interpretation of the experimental data, although our simulation cell, consisting of PS tetramers adsorbed on a silver surface (Fig. 1), does not appear a straightforward model of the sample studied in the experiments. Care will be taken, however, not to explain the experimental trends by a literal interpretation of the simulation results.

In Section 3, we first show that the disappearance cross-sections vary with the size of the fragments and we discuss the real meaning of this parameter, in connection with damage and ejection area. Then we show that the kinetic energies of charged PS fragments are also correlated to the

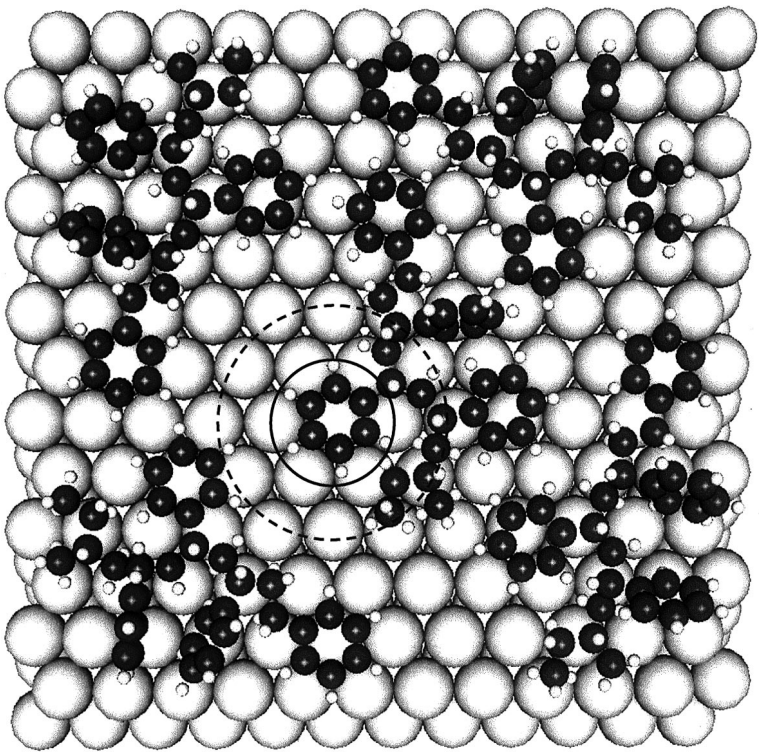

Fig. 1. Top view of the simulation cell used for the bombardment of polystyrene molecules by 500 eV Ar atoms. The full circle corresponds to the calculated ejection area of the phenyl radical and the dashed circle represents the experimental disappearance cross-section of the same fragment.

fragment size and to characteristic radii derived from the disappearance cross-sections. The meaning of these correlations is discussed in detail and, in particular, their relevance to explain the distribution of energy on the bombarded sample surface. Our results are finally compared to other reported data for keV bombardment of organic monolayers on metals and for 72.3 MeV ^{127}I ion bombardment of PVDF [1].

2. Materials and methods

2.1. Samples

The polystyrene, C_4H_9–$[C_8H_8]_n$–H (number average molecular weight, $M_n = 60\,000$; polydispersity, $H = 1.05$), is dissolved in toluene. The samples are prepared as thin films cast on silicon substrates (1 cm^2), by depositing a droplet of the solution on the supports. Prior to deposition, the substrates are rinsed in water of HPLC grade from a milli-Q system (Millipore), isopropanol and hexane. The low concentration of the solutions allows us to deposit thin polymer layers, ensuring a sufficient electric contact between the top surface and the sample holder. In this way, charging effects can be avoided. This procedure has been fully described in [15,16]. The reduction of the silicon signal by two orders of magnitude in comparison with clean silicon surfaces indicates that the average polymer layer thickness should be close to 50 Å [17]. All the energy measurements are conducted with samples respecting these requirements. Such samples can be reproducibly built up from carefully dosed PS solutions. In the discussion, acetylene (C_2H_2), butyl (C_4H_9) and phenyl (C_6H_5) ions will be referred to either by their name or formula.

2.2. ToF-SIMS setup

The secondary ion mass analyses, ion beam degradation and KED measurements are performed in a PHI-EVANS Time-of-Flight SIMS (TRIFT 1) using a pulsed $^{69}Ga^+$ beam (FEI 83-2 liquid metal ion source with 15 keV energy; ~400–800 pA DC current; 24 ns pulse width bunched down to 1.2 ns; 5 kHz repetition rate) [18]. The angle between the primary ion source and the spectrometer axes (perpendicular to the surface) is 35°. Due to the strong electric field in front of the sample surface, which is maintained at a potential of 3 kV for secondary ion acceleration, the resulting impact energy and angle in the positive ion detection mode are 12 keV and 40°, respectively. After emission, the accelerated secondary ions, having 3 keV kinetic energy at the grounded extractor that forms part of the immersion lens, are focused by the immersion lens and transported via a transfer lens. They are then deflected 270° by three hemispherical electrostatic analyzers (ESA) before reaching the detector (fast dual microchannel plate). In the nominal analysis conditions, ToF-SIMS spectra in the mass range $0 < m/z < 5000$ are obtained from 300 s acquisitions on a 130×130 μm^2 sample area, leading to a primary ion fluence (F) close to 10^{12} ions/cm^2.

2.3. Ion beam damage measurements

For polymer surface degradation studies, continuous bombardments on a larger area (190×190 μm^2) with the same $^{69}Ga^+$ source are alternated with routine ToF-SIMS analysis periods [19] in order to reach a maximum fluence of 5×10^{14} ions/cm^2.

2.4. KED measurements

To obtain the energy spectra, a+$(3000 - \Delta)$ V potential is applied to the sample. At the crossover following the first ESA, where the energy dispersion is maximum, the secondary ions are energy selected by a 100 μm slit (1.5 eV passband). The acquisition of mass spectra on the same sample area but for different sample voltages (different Δ) allows us to collect the signal corresponding to different energy windows of the KED, a 1 V increase of the sample potential corresponding to a 1 eV decrease in the KED. In order to avoid polymer degradation [19] and surface charging during these experiments, several sets of measurements are conducted on different areas and the energy slit is slightly shifted between successive sets of measurements. By this means, the whole energy spectrum is scanned with enough accuracy. In

another set of experiments, the KED is measured with a constant sample voltage, by moving the energy slit in order to select different energy windows. The position of the slit is then mathematically converted into energy via an equation derived from the calculation of the ion trajectories in the TRIFT spectrometer [20]. To combine the different sets of measurements, the zero of the energy scale for each set is estimated from the intersection V_o between the tangent to the increasing part of the KED of atomic ions and the voltage axis. The initial kinetic energy E_k of the secondary ions is thus obtained using $E_k = e(V_0 - 3000 + \Delta)$. Because unimolecular decomposition reactions in the linear part of the spectrometer can give rise to negative values of E_k [15,16,21], this quantity is preferably called 'apparent kinetic energy' in the following discussion.

2.5. Molecular dynamics simulations

The Ar bombardment of sec-butyl terminated polystyrene tetramers adsorbed on an Ag(1 1 1) surface is modeled using molecular dynamics (MD) computer simulation. The details of the simulation have been described elsewhere [14]. Briefly, the sample consists of 5 PS tetramers placed on the Ag{1 1 1} surface (9 layers of 156 atoms each). Fig. 1 shows a top view of the simulation cell. The entire system is quenched to a minimum energy configuration prior to Ar atom impact. A total of 4000 Ar trajectories directed along the surface normal were calculated. The simulation consists of integrating Hamilton's equations of motion over some time interval to determine the position and velocity of each particle as a function of time. The energy and forces in the system are described by many-body interaction potentials, in particular, the C–C, C–H and H–H interactions are described by the Brenner potential function [22,23]. One important feature of this potential is that it allows for chemical reaction and accompanying changes in atomic hybridization during the course of a reaction. The criterion for terminating the trajectory is that the total energy of any atom is too low to induce ejection. The termination times range from 0.5 to 6 ps, depending on the impact point of the primary particle and the manner in which the energy distributes within the solid. Experimentally observable properties, such as total yield, mass spectrum, kinetic energy and angular distributions are calculated from the final positions, velocities and masses of all the ejected species. Mechanistic information is obtained by monitoring the time evolution of relevant collisional events.

3. Results and discussion

In the first part of the results (Section 3.1), the question of the damage at the surface of bombarded PS is addressed in detail. The degradation laws and disappearance cross-sections of hydrocarbon ions sputtered from PS are presented and shown to depend on the fragment nature. This leads us to question the real meaning of the disappearance cross-section. To explain the observed variation, we propose, with the help of MD simulations, a simple picture in which the disappearance cross-section and ejection radii correlate with the size of the fragments because the average damage area is smaller or similar to the fragment size. In turn, it is also demonstrated that the disappearance cross-sections provide a reasonable estimate of the ejection area of the fragments. In the second part of the results (Section 3.2), we present experimental data showing that the kinetic energy of the fragments is also connected to their size. Several arguments are developed to support the hypothesis that the kinetic energies mirror the local energy density giving rise to ejection. Therefore, the correlation between kinetic energies of the ejected fragments and disappearance radii provides a realistic estimate of the energy profile around the impact point.

3.1. Correlation of damage cross-section with ejection radius

3.1.1. Disappearance cross-section

When a polymer surface is irradiated by keV ions with fluences higher than 10^{12} ions/cm^2, damage starts to develop so that any subsequent static SIMS analysis not only scans pristine material but also damaged regions [24]. Consequently,

the secondary ion yields gradually change with increasing primary ion fluence, and are thus a sensitive probe of the physico-chemical modification of the surface [25–28]. During the bombardment process, the intensity of the characteristic fragment ions, i.e., resulting from one or two C–C bond scissions and, sometimes, H atom addition, usually exhibits a monotonic decay. By contrast, the intensity of degradation products tends to increase [19,29,30]. The intensity of extensively fragmented ions which arise from both the original and the damaged structures often undergo a maximum followed by a smooth decay. For the most characteristic ions that are not induced by the degradation, the intensity decay $I_i(\phi)$ can be fit with a simple exponential function,

$$I_i(\phi) = I_{i0} \exp(-\sigma_i \phi), \quad (1)$$

where ϕ is the primary ion fluence and I_{i0} is the extrapolated intensity of fragment i at zero fluence. In Eq. (1), σ_i is defined as the disappearance cross-section of fragment i.

To illustrate the concept, Fig. 2(a) reports the evolution of several PS ion intensities as a function of the primary ion fluence in the first stages of the degradation. As soon as the sample is irradiated, the absolute intensities of these ions start to decrease. The decay is more pronounced for large fragments which mirror the polymer structure ($C_8H_8^+$) than for small hydrocarbons ($C_2H_2^+$). Nevertheless, all the degradation curves shown in Fig. 2(a) can be reasonably fit by a single exponential function. Thus, the production of similar ions induced by the degradation should be negligible. Some of the other hydrocarbon ions sputtered from PS do not exhibit such a straightforward behavior. In particular, the intensities of C^+, CH_2^+, CH_3^+ and C_2^+ first increase with the primary ion fluence in this range. These ions are not taken into account for the evaluation of the disappearance cross-sections since their fluence dependencies indicate more complex mechanisms than a straightforward, gradual disappearance of the precursor. The disappearance cross-sections σ_i provided by the fit of the experimental curves (Fig. 2(a)) are plotted as a function of the fragment mass in Fig. 2(b). The disappearance cross-sections range from

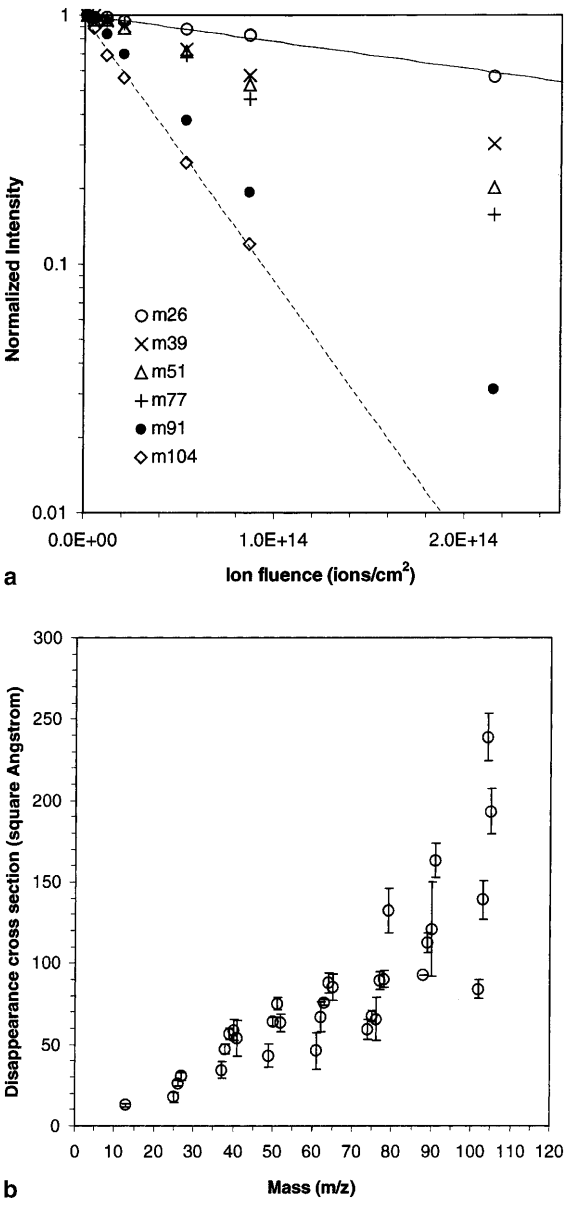

Fig. 2. (a) Dependence of the polystyrene peak intensities on the cumulated $^{69}Ga^+$ (15 keV) ion fluence. (b) Disappearance cross-sections (Å^2) of the hydrocarbon fragments sputtered from polystyrene as a function of the fragment mass.

$\sim$13 Å^2 for CH^+ to $\sim$240 Å^2 for $C_8H_8^+$. Although the distribution of disappearance cross-sections suggests a predominant influence of the fragment mass, there is also a variation related to the number of H atoms in the molecule.

3.1.2. Interpretation of the disappearance cross-section

Different meanings have been implicitly attributed to the disappearance cross-sections by various authors, including the average surface area damaged by a single ion and the average ejection area of the sputtered species. A basic definition of the disappearance cross section is *the average area per incident particle from where ejection of the corresponding fragment is excluded*. This exclusion can be caused by any kind of irreversible damage to the fragment precursors in the area or by the ejection of the precursors as a part or as a whole. The disappearance cross-section σ is therefore influenced by the sputtering yields of all the fragments and by the rate of creation of any sort of damage on the sample surface (bond-breaking, implantation, reactions). The variation of σ for different fragments indicates that σ cannot be directly related to a single global quantity of damage per incident particle.

Under certain assumptions, the excluded area determined by the disappearance cross-section should mirror the ejection area. For instance, if there is no other damage than that related to fragment ejection, the excluded area σ of the fragments should include their ejection area. In contrast, if other damage mechanisms predominate and if their distribution extends on a much greater area than the ejection area, then the disappearance cross-sections might be much larger and unrelated to ejection radii. For keV particle bombardment of organic molecules, these two cases seem quite unrealistic. More reasonable would be a scenario in which damage unrelated to ejection is significant, but where the area affected by this type of damage is smaller or roughly equivalent to the ejection area. In this case, the influence of the ejection should be predominant, and the disappearance cross-sections is expected to correlate with the ejection radii.

There is another important particularity related to keV particle bombardment. Indeed, the disappearance cross-sections are not much larger than the fragment sizes, and if the areas undergoing damage or particle ejection are reasonably close or smaller than the size of the considered fragments, another effect comes into play. For example, damage caused by the implantation or ejection of a surface carbon atom will prevent the ejection of the phenyl to which it initially belongs, but not the ejection of acetylene from the same phenyl ring (same area). In other words, this kind of damage will automatically induce a dependence of the disappearance cross-section on the size of the ejected fragment. Such dependence is indeed observed in Fig. 2(b). In contrast, in the MeV bombardment results described in [1], the disappearance cross-sections are much larger than the fragment size, and they indeed show little influence of the fragment size. To establish the existence of a correlation between σ and the ejection area, inaccessible to experiment, we can rely on the realistic model provided by MD simulation.

3.1.3. Ejection radius

The distributions of distances between the impact point and the center of mass of the ejected fragments, as calculated in the simulation, are shown in Fig. 3. By definition, the curves of Fig. 3 constitute *distributions* of ejection radii. The first

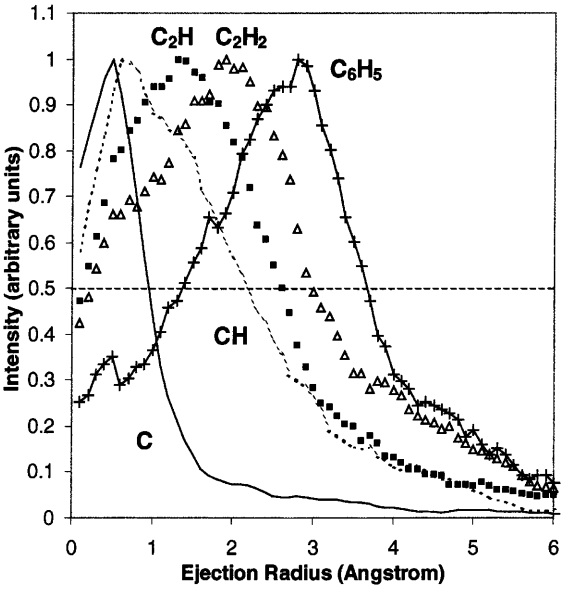

Fig. 3. Calculated distributions of distances between the impact point and the center-of-mass of the nascent fragments obtained from MD simulations (500 eV Ar bombardment of polystyrene tetramers adsorbed on silver).

information provided by the MD simulation is that there is not a single ejection radius for a given fragment, but a distribution of ejection radii, whose width varies for different fragments. The shape of these distributions can be explained by the analysis of the trajectories. Movies of the action show that the ejection of hydrocarbon fragments is mostly induced by the direct interaction between the primary particle and the tetramer backbone [14,31,32]. As predicted earlier by Leggett and Vickerman [33], the role of this initial interaction is to cause a first bond-scission in the chain, thereby making one end of the nascent fragment free. To eject the fragment, a second bond scission is induced by a moving C atom or by rotational and vibrational excitation in the considered chain segment [14,31]. As corollary, the ejection area surrounds the impact point in most cases. Another consequence of this mechanism, where the primary particle brings downward momentum and causes damage at the impact, is that the ejection radius distribution of the ejected species is depleted at the position of impact. The fact that the distance between the impact and the maximum of the distribution, i.e., the size of the depleted region around the impact, is correlated to the fragment size is again explained by the very small lateral extent of the damage for these bombardment conditions. Using the same example as before, the implantation or ejection of a carbon right at the impact will prevent the ejection of other fragments from an area that is proportional to their size. For comparison with the experimental values of disappearance cross-sections, we need to extract one single characteristic value of ejection radius that characterizes best the whole distributions. The radius value corresponding to the maximum of the distributions seems the most reasonable choice.

3.1.4. Correlation between disappearance cross-section and ejection radius

A plot of the radii derived from experimental disappearance cross-sections $r_i = (\sigma_i/\pi)^{0.5}$ as a function of the calculated ejection radii for several fragments observed in the simulation and in the experiment is given in Fig. 4. There is a clear correlation between the two sets of values and the

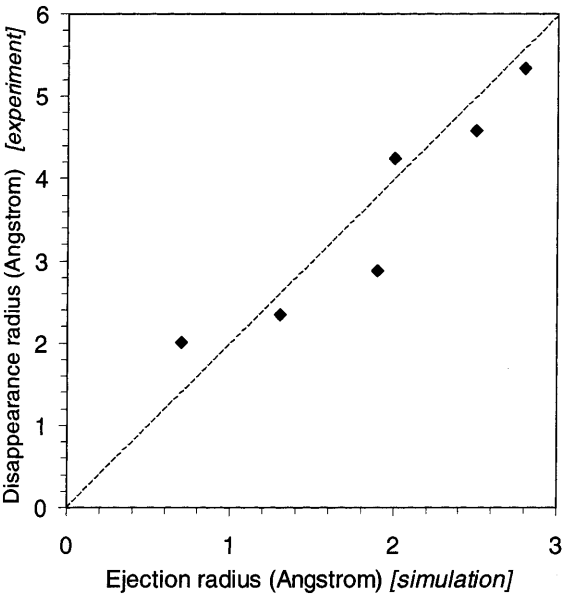

Fig. 4. Correlation between the disappearance radii (experiment) and ejection radii (simulation).

intercept of the best linear regression through the data is very close to zero. Therefore, in agreement with our previous assumptions, it appears reasonable to use the radii derived from the disappearance cross-section as an estimate of the ejection radii. Nevertheless, the slope of the regression line of Fig. 4 is two, and not one. The reason of this discrepancy can be tentatively explained. In Fig. 1, the calculated ejection area (full circle) and the disappearance cross section of C_6H_5 (dashed circle) have been superimposed to the top view of the simulation cell. The ejection area of the phenyl is very close to the area occupied by the molecule on the surface. Using Fig. 1 as an illustration, it is easy to envision that the ejection of the marked phenyl will prevent any further ejection of other phenyl rings in a radius which corresponds roughly to its disappearance cross-section. The same observation can be done for other fragments. It is interesting to note that the disappearance cross-sections should depend on the concentration of the fragment precursors on the surface, while the ejection radii should not. Therefore, the slope of the curve in Fig. 4 should depend on the considered system. In this respect, the fact that the

systems analyzed in the SIMS experiments and in the MD simulations are slightly different might also introduce a bias in the correlation and the value of the slope should not be taken as an accurate number.

Although the details of the ejection processes might be different in the MD simulation and in the present experiment because the samples and the bombardment conditions are not exactly the same, we believe that the role of the primary particle and the major trend indicated by the simulation are likely to remain. In this respect, calculations performed at 5 keV suggest that the primary beam energy does not significantly influence the fragmentation mechanism [34]. Accordingly, the radius $r_i = (\sigma_i/\pi)^{0.5}$ really mirrors the average distance between the primary impact point and the nascent fragment *i*.

3.1.5. Comparison with MeV ion data

There are several differences between our data related to keV particle bombardment and the results reported by Papaleo et al. [1] for 55 MeV ^{127}I bombardment of PVDF. First, the keV disappearance cross-sections are one or two orders of magnitude smaller than those obtained under MeV ion excitation. The area per incident particle from which ejection is excluded by a single MeV ion is thus 10–100 times larger than for a keV ion. Second, the MeV ion bombardment data do not seem to exhibit the predominant influence of the fragment size observed under keV ion bombardment, as mentioned before. Instead, the variation related to the hydrogen content of the fragments is dramatic even for small fragments. Thus, the damage induced by electronic MeV ion excitation of the target is spread on a much larger area and it mainly causes an increasing dehydrogenation when going from the periphery to the inner core of the track [35].

3.2. Correlation of energy distribution with ejection radius

3.2.1. Width of the kinetic energy distributions

The kinetic energy distributions (KED) of hydrocarbon ions sputtered from PS were repeatedly measured using fresh samples and slightly different variants of the experimental procedure (see the Experimental Section). The data are illustrated by the inset of Fig. 5, showing the KEDs of ions with six C atoms and two to seven H atoms recorded in a single set of measurements. The FWHMs of the distributions are chosen as characteristic numbers to describe the kinetic energies of the sputtered species. Indeed, they are directly proportional to the median of the KEDs for such C_xH_y fragments [36]. As stated in previous articles [15,16,37,38], the kinetic energies of the hydrocarbon fragments sputtered from various organic films including PS are influenced by two major factors. First, the average kinetic energy transferred to the fragment decreases with increasing fragment size. This trend is clearly indicated in Fig. 5 by the relatively high energies measured for some of the small fragments (C_2H^+, $C_2H_2^+$, C_3H^+, C_4H^+) in comparison with the low energies of most of the large ions (beyond 80 amu). Second, there is a variation of the FWHMs related to the hydrogen content of the fragments [38]. Among ions containing the same number of C atoms, strongly unsaturated species have larger kinetic energies than fragments containing more hydrogen (inset of Fig. 5). This chemical effect leads to a periodic pattern in the energy versus mass plot of Fig. 5. The connection between the kinetic and formation energies of hydrocarbon ions has been investigated in [36]. For comparison, measurements of the radial velocities of the ejected species in MeV bombardment of polymers indicate that the kinetic energies are predominantly influenced by the chemical effect (hydrogen content) and not by the size effect [1,35,39]. In the following section, we show that the kinetic energy of the fragments can be used as an estimate of the local energy density in the region of emission. It is indeed possible to derive a relationship between these two parameters using analytical expressions and MD results.

3.2.2. Connecting kinetic energy and local energy density

The local energy density at the surface is the total energy E per unit volume in the surface layer [40]. Beyond the size of the C–H unit, i.e., above the atomic level, the mass of a PS fragment is proportional to its volume. Therefore, the local

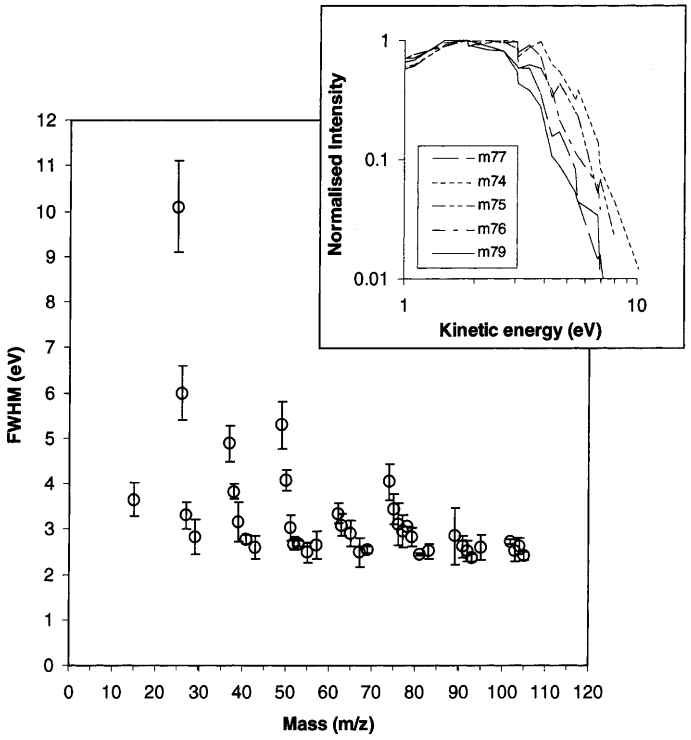

Fig. 5. Characteristic widths of the kinetic energy distributions for hydrocarbon fragments sputtered from polystyrene. Inset: energy spectra of ions containing six carbon atoms.

energy density ε can be reasonably expressed as the total energy per unit mass (eV/amu). If the considered species is a nascent fragment of mass M, according to our definition, the energy density in the fragment precursor is equal to

$$\varepsilon = E/M. \tag{2}$$

The relationship between the total energy E of a fragment and its kinetic energy E_k must still be established. In a phenomenological model describing the characteristic kinetic energy of sputtered hydrocarbon ions [36], we used simple equations to express the partition of the transferred energy into internal and kinetic energies of the nascent fragment [41,42].

$$E_k = m_1/(m_1 + m_2)E, \tag{3}$$

$$E_{rel} = m_2/(m_1 + m_2)E, \tag{4}$$

where E_{rel} is the internal energy (vibration and rotation) transferred to the fragment. In this treatment, the fragment is divided into two subunits of mass m_1 and m_2 with $m_1 + m_2 = M$. The mass m_1 corresponds to the part of the fragment to which the momentum is initially transferred and m_2 is the mass of the part of the fragment that does not directly receive momentum. In this simple picture, m_1 is immediately set in motion while m_2 is still at rest. These equations account for the influence of the size of hydrocarbon fragment on the observed kinetic energies [36]. Interestingly, Eqs. (3) and (4) involve a linear correlation between E_k and E_{rel} that depends on the mass of the considered fragment.

Blending Eqs. (2) and (3) directly leads to a new expression of the kinetic energy E_k of the departing fragment as a function of the energy density ε at the surface.

$$E_k = m_1\varepsilon. \tag{5}$$

If the emission of the considered hydrocarbon fragments is induced by the same type of local

atom–atom interaction, m_1 is constant. For instance, $m_1 = 12$ if the momentum is primarily transferred to a single C atom. Then the kinetic energy of the fragments is directly proportional to the local energy density inducing the sputtering event. This analysis is, of course, an oversimplified view but it serves as a starting point for the discussion below.

Although molecular dynamics modeling of the ejection of C_xH_y fragments from PS tetramers indicates that these concepts are probably too simple [14], a correlation between E_k and E_{rel} is also observed in the simulations and it is indeed strongly influenced by the fragment/molecule mass [12,14,31]. More quantitatively, our new simulation results allow us to check the validity of Eq. (5), using the distributions of kinetic energy (E_k) and total energy (E) of the fragments. If the above equations are valid, one should observe a linear correlation between the characteristic values of E_k and E/M. Again, the FWHM of the energy distributions can be used as characteristic values to describe the kinetic and total energies of the fragments. The correlation between E_k and E/M is plotted in Fig. 6 for the most intense C_xH_y fragments observed in the simulation. The line $y = 13x$, which corresponds to the best linear regression, is superimposed to the data points as a guide for the eye. Actually, the linear regression constitutes a very good approximation of the relationship between E_k and E, especially for small fragments containing up to five C atoms. For larger fragments, the relation changes gradually, and the kinetic energies tend to form a plateau (three data points on the left). Nevertheless, Fig. 6 demonstrates that our simple analytical expression (Eq. (5)) describes the behavior of C_xH_y sufficiently well. According to Eq. (5), the fact that the slope of best linear regression is close to 12 suggests that the momentum which causes fragment ejection is primarily transferred to one single carbon atom belonging to the fragment. This is indeed the most frequent scenario observed in the movies from the MD simulations.

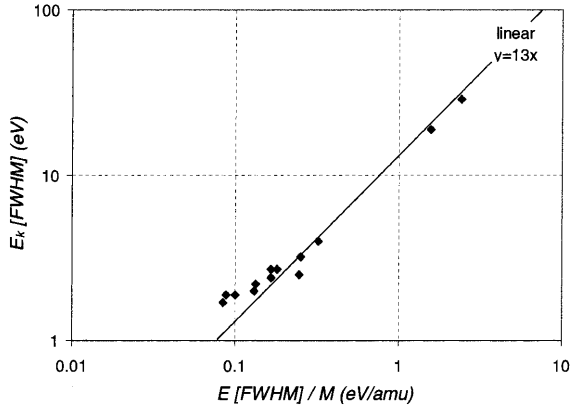

Fig. 6. Correlation between E_k and E/M for C_xH_y species sputtered from polystyrene molecules adsorbed on silver (MD simulations).

3.2.3. Correlation between kinetic energy and disappearance radii

The relation between disappearance radius $r_i = (\sigma_i/\pi)^{0.5}$ and ejection radius has been established in Section 3.1, as well as the relation between kinetic energy and local energy density in Section 3.2. Therefore, connecting the kinetic energies of the sputtered species to the estimate of the ejection radius provided by the disappearance cross-sections should provide an average profile of the energy deposition at the surface. In Fig. 7, the FWHMs of the energy distributions (Fig. 5) are plotted as a function of the radii r_i derived from the disappearance cross-sections (Fig. 2(b)). Fig. 7 indicates that there is indeed a correlation between the data determined from the two independent sets of measurements. The curve of Fig. 7 mirrors the average profile of the energy deposited in and around the damaged area. The energy decreases steeply up to 5 Å and forms a plateau beyond this value. The asymptotic behavior of the kinetic energies beyond 5 Å might be partly due to the energy resolution of the slit, experimentally limited to 1.5 eV (dashed line in Fig. 7), and partly to the kinetic energy threshold also observed in the MD results for large fragments (Fig. 6). Considering the profile of Fig. 7, it is important to keep in mind that the disappearance radius $r_i = (\sigma_i/\pi)^{0.5}$ probably overestimates the ejection radius by a factor of 2. Therefore, the energy profile should be even narrower, indicating that the energy causing the ejection is distributed among the few atoms surrounding the impact. It is also useful to remind

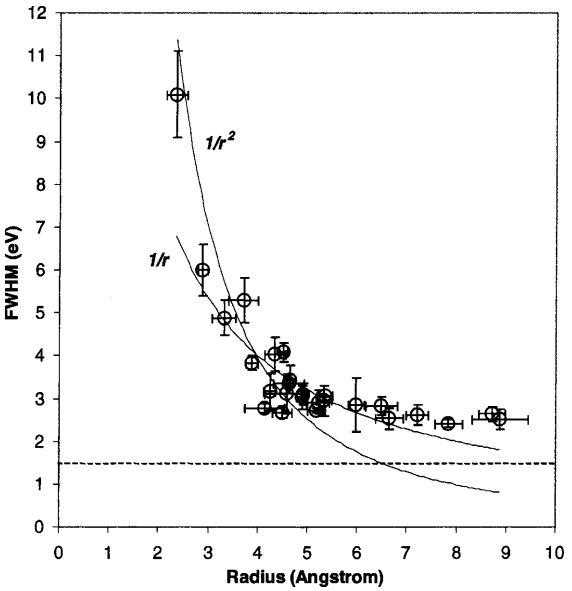

Fig. 7. Correlation between the widths of the kinetic energy distributions and the damage radii for hydrocarbon fragments sputtered from polystyrene.

that the energy profile beyond 2 Å, as shown in Fig. 7, corresponds to upward momentum transfer inducing ejection. In contrast, the energy profile below this distance, inaccessible to experiment, should mostly reflect the downward momentum of the primary particle.

The interpretation of the correlation of Fig. 7 as a picture of the energy profile at the surface of the bombarded sample can be further validated by MD simulation results. In this respect, Fig. 8 shows the kinetic energies of sputtered C atoms as a function of the distance between their center-of-mass and the impact point in the MD simulation of 500 eV Ar sputtering of PS tetramers. Due to their size, one can consider that sputtered C atoms really probe the local energy density at the position they belong before ejection. Although the ejection of C atoms is only a probe of the most energetic fraction of the ejection events and, therefore, cannot provide an average energy profile on all the possible events, the similarity of the profiles in Figs. 7 and 8 is interesting and supports our interpretations. Another interesting feature of this profile is that it gives access to the energies at very short distances from the impact, below 3 Å. Fig. 8

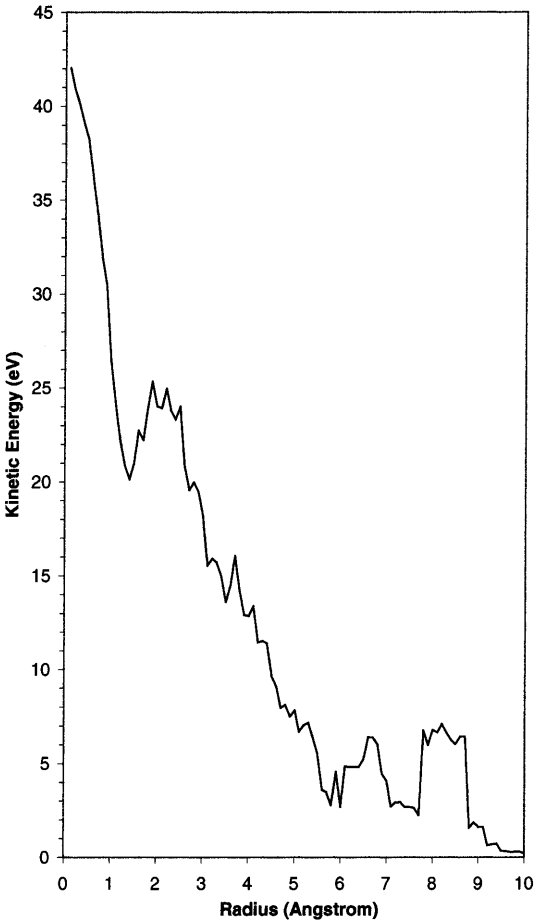

Fig. 8. Calculated kinetic energy of the sputtered C atoms as a function of the distance from the impact point in the MD simulations of 500 eV Ar bombardment of polystyrene molecules adsorbed on silver.

shows that the transferred energy may be much higher at the very impact point than at the shortest distance probed by the experiment. In conclusion, the energy profiles suggested on the independent grounds of the MD simulation and of the experiment agree reasonably well, thereby providing broader insights into the energy deposition induced by keV particles in organic layers.

3.2.4. Comparison with other experimental data

There are several reports from the Münster group concerning the determination of the deposited energy profile around the impact point in

keV ion bombardment of Ni and Au surfaces covered by small molecules [9,10]. These studies suggest that the impact energy is confined in a radius of 10 Å around the impact point. In addition, the energy profiles show the characteristic $1/r^n$ dependence as observed in Fig. 7. In contrast with our measurements though, the characteristic energy values on the *Y*-axis of these profiles are derived from thermal desorption measurements. Therefore, they should constitute a lower limit of the energy involved in the sputtering process. The different approach used in our paper explains the higher kinetic energy values in Fig. 7. Remarkably, our energy values lie in the same range as those measured by Papaleo et al. [1] with a similar procedure but for MeV excitation energies. The comparison with the energy profile obtained under 72.3 MeV ^{127}I bombardment of PVDF brings additional information. First, the shape of the profile is similar under keV and MeV ion bombardment. Second, the profile is 5 times broader in the case of MeV irradiation. The dilatation of the profile along the radius axis for MeV ion bombardment is consistent with the much larger stopping power in this energy range (~655 eV/Å for 72.3 MeV ^{127}I versus ~84 eV/Å for 12 keV ^{69}Ga).

4. Conclusion

The combination of ion-induced degradation studies, energy distribution measurements and MD simulations provides insights into both the extent of the damaged area and the energy transfer in this region. First, the disappearance cross-sections of hydrocarbon fragments sputtered from keV ion bombarded polystyrene are correlated to the size of the ejected species. Molecular dynamics results indicate that the disappearance and ejection radii are correlated in a given system. Second, the kinetic energies of the sputtered fragments mirror the energy transfer leading to their ejection and simple arguments, supported by MD results, suggest that they are directly connected to the local energy density at the desorption point. Therefore, the correlation between kinetic energies and disappearance radii of the fragments provides an estimate of the deposited energy profile at the surface of the bombarded sample. A similar profile can be deduced from MD simulations. In agreement with the respective stopping powers, the energy profile obtained under 12 keV ^{69}Ga ion sputtering of PS is 5 times narrower than that corresponding to 72.3 MeV ^{127}I ion bombardment of PVDF.

Acknowledgements

The authors thank Bruno Schueler and Fraser Reich from PHI-EVANS for their help and advice concerning the KED measurements, as well as Xavier Vanden Eynde for helpful discussion concerning the sputtering of PS. Ricardo Papaleo is gratefully acknowledged for reading and commenting the manuscript. AD is also indebted to Kristin Krantzman for stimulating ideas concerning the energy profile at the sample surface during keV ion bombardment. The financial support of the National Science Foundation through the Chemistry Division, the CRIF program and the MRI program are gratefully acknowledged by AD and BJG. Additional computational resources were provided in part by the IBM Selected University Resource Program and the Center for Academic Computing of Penn State University. We are also indebted to the Center for Academic Computing staff for helping us use the IBM SP computer and for the development of a new graphics software for animation and presentation. The experimental part of this work is supported by the *Action de Recherche Concertée* (94/99–173) of the *Communauté Française de Belgique* and by the Belgian Interuniversity Attraction Pole Program (PAI-IUAP P4/10) on Reduced Dimensionality Systems. BGS is supported by a grant from the Belgian *Administration Générale de la Coopération au Développement*. The ToF-SIMS equipment was acquired with the support of the *Région Wallonne* and *FRFC-Loterie Nationale* of Belgium.

References

[1] R.M. Papaleo, P. Demirev, J. Eriksson, P. Hakansson, B.U.R. Sundqvist, R.E. Johnson, Phys. Rev. Lett. 77 (1996) 667.

[2] G.J. Leggett, J.C. Vickerman, Int. J. Mass Spectrom. Ion Processes 122 (1992) 281.
[3] P.A. Demirev, Mass Spectrom. Rev. 14 (1995) 279.
[4] A. Benninghoven, F.G. Rüdenauer, H.W. Werner, Secondary Ion Mass Spectrometry, Wiley, New York, 1987.
[5] G. Gillen, R. Lareau, J. Bennett, F. Stevie (Eds.), Secondary Ion mass Spectrometry, SIMS XI Proceedings, Wiley, New York, 1998.
[6] The Twelfth International Conference on Secondary Ion Mass Spectrometry (SIMS XII), Brussels, 5–10 September 1999.
[7] A. Benninghoven, in: A. Benninghoven, J. Giber, J. Laszlo, M. Riedel, H.W. Werner (Eds.), Secondary Ion mass Spectrometry, SIMS III Proceedings, Springer, Berlin, 1982, p. 438.
[8] A. Benninghoven, in: A. Benninghoven (Ed.), Ion Formation from Organic Solids, Springer Series in Chemical Physics, Vol. 25, Springer, Berlin, 1983, p. 77.
[9] D. Greifendorf, P. Beckmann, M. Schemmer, A. Benninghoven, in: A. Benninghoven (Ed.), Ion Formation from Organic Solids, Springer Series in Chemical Physics, Vol. 25, Springer, Berlin, 1983, p. 118.
[10] D. Rading, R. Kersting, A. Benninghoven, in: G. Gillen, R. Lareau, J. Bennett, F. Stevie (Eds.), Secondary Ion mass Spectrometry, SIMS XI Proceedings, Wiley, New York, 1998, p. 455.
[11] R.S. Taylor, B.J. Garrison, Langmuir 11 (1995) 1220.
[12] R. Chatterjee, Z. Postawa, N. Winograd, B.J. Garrison, J. Phys. Chem. B 103 (1999) 151.
[13] K.S.S. Liu, C.W. Yong, B.J. Garrison, J.C. Vickerman, J. Phys. Chem. B 103 (1999) 3195.
[14] A. Delcorte, X. Vanden Eynde, P. Bertrand, J.C. Vickerman, B.J. Garrison, J. Phys. Chem. B 104 (2000) 2673.
[15] A. Delcorte, B.G. Segda, P. Bertrand, Surf. Sci. 381 (1997) 18.
[16] A. Delcorte, B.G. Segda, P. Bertrand, Surf. Sci. 389 (1997) 393.
[17] A. Delcorte, P. Bertrand, X. Arys, A. Jonas, E. Wischerhoff, B. Mayer, A. Laschewsky, Surf. Sci. 366 (1996) 149.
[18] B.W. Schueler, Microsc. Microanal. Microstruct. 3 (1992) 119.
[19] A. Delcorte, L.T. Weng, P. Bertrand, Nucl. Instr. and Meth. B 100 (1995) 213.
[20] B.W. Schueler, Private communication.
[21] A. Delcorte, P. Bertrand, Int. J. Mass Spectrom. 184 (1999) 217.
[22] D.W. Brenner, Phys. Rev. B 42 (1990) 9458.
[23] D.W. Brenner, J.A. Harrison, C.T. White, R.J. Colton, Thin Solid Films 206 (1991) 220.
[24] S. Pignataro, Surf. Interface Anal. 19 (1992) 275.
[25] D. Briggs, A.B. Wooton, Surf. Interface Anal. 4 (1982) 109.
[26] J.A. Van den Berg, Vacuum 36 (1986) 981.
[27] D. Briggs, M.J. Hearn, Vacuum 36 (1986) 1005.
[28] G.J. Leggett, J.C. Vickerman, Anal. Chem. 63 (1991) 561.
[29] J.-B. Lhoest, J.-L. Dewez, P. Bertrand, Nucl. Instr. and Meth. B 105 (1995) 322.
[30] I.S. Gilmore, M.P. Seah, Surf. Interface Anal. 24 (1996) 746.
[31] A. Delcorte, P. Bertrand, J.C. Vickerman, B.J. Garrison, in: Secondary Ion mass Spectrometry, SIMS XII Proceedings, 2000.
[32] T.C. Nguyen, D.W. Ward, J.A. Townes, A.K. White, K.D. Krantzman, J. Phys. Chem. (2000) in press.
[33] G.J. Leggett, J.C. Vickerman, Int. J. Mass Spectrom. Ion Proc. 122 (1992) 281.
[34] A. Delcorte, B.J. Garrison, J. Phys. Chem. B (2000) in press.
[35] R.M. Papaleo, Nucl. Instr. and Meth. B 131 (1997) 121.
[36] A. Delcorte, P. Bertrand, Nucl. Instr. and Meth. B 117 (1996) 235.
[37] A. Delcorte, P. Bertrand, Nucl. Instr. and Meth. B 115 (1996) 246.
[38] A. Delcorte, P. Bertrand, Nucl. Instr. and Meth. B 135 (1998) 430.
[39] R.M. Papaleo, P. Demirev, J. Eriksson, P. Hakansson, B.U.R. Sundqvist, Phys. Rev. B 54 (1996) 3173.
[40] T. Nguyen, D. Ward, J.A. Townes, A.K. White, K.D. Krantzman, B.J. Garrison, in: Secondary Ion mass Spectrometry, SIMS XII Proceedings, 2000.
[41] K. Snowdon, Nucl. Instr. and Meth. B 9 (1985) 132.
[42] P. Sigmund, H.M. Urbassek, D. Matragrano, Nucl. Instr. and Meth. B 14 (1986) 495.